## REFERENCES AND NOTES

1. D. S. Bethune *et al.*, *Nature* **363**, 605 (1993).
2. S. Iijima and T. Ichihashi, *ibid.*, p. 603.
3. M. S. Dresselhaus, G. Dresselhaus, P. C. Eklund, *Science of Fullerenes and Carbon Nanotubes* (Academic Press, New York, 1996).
4. A. Thess *et al.*, *Science* **273**, 483 (1996).
5. R. E. Smalley *et al.*, unpublished results.
6. P. C. Eklund, J. M. Holden, R. A. Jishi, *Carbon* **33**, 959 (1995).
7. J. M. Holden *et al.*, *Chem. Phys. Lett.* **220**, 186 (1994).
8. H. Hiura, T. W. Ebbesen, K. Tanigaki, H. Takahashi, *ibid.* **202**, 509 (1993).
9. N. Chandrabhas *et al.*, *Pramana J. Phys.* **42**, 375 (1994).
10. J. Kastner *et al.*, *Chem. Phys. Lett.* **221**, 53 (1994).
11. Carbon arc synthesis can also produce MWNTs, which have been shown by TEM to consist of many concentric SWNTs. Each MWNT contains typically between 10 to 20, and as many as 100, concentric tubules with an intertubule spacing of ~3.4 Å. A typical inner diameter for a MWNT is ~8 nm, a factor of ~6 greater than the SWNTs studied here. These MWNTs are too large to exhibit strong quantum-confinement effects, and the Raman spectrum for MWNTs resembles closely that of graphite. See, for example, (*6*).
12. A. M. Rao *et al.*, unpublished results.
13. As discussed in (*4*), the laser-assisted production of SWNTs creates crystalline ropes containing bundles of aligned SWNTs. The tubules stack in a close-packed structure. When viewed end on, the tube ends form a triangular lattice whose lattice parameter has been observed with x-ray and electron diffraction.
14. The TEM was calibrated by using the lattice-fringe spacing from graphite (3.35 Å).
15. Because the Raman spectra presented in this report were collected with a wide range of laser frequencies, several spectrometers and varying collection optics were needed.
16. L. Venkataraman, thesis, Massachusetts Institute of Technology (1993).
17. R. A. Jishi, L. Venkataraman, M. S. Dresselhaus, G. Dresselhaus, *Chem. Phys. Lett.* **209**, 77 (1993).
18. E. Richter and K. R. Subbaswamy, unpublished results.
19. J. M. Cowley, P. Nikolaev, A. Thess, R. E. Smalley, preprint.
20. C. H. Xu, C. Z. Wang, C. T. Chan, K. M. Ho, *J. Phys. Cond. Matter* **4**, 6047 (1992).
21. Y. H. Lee, M. S. Kim, D. Tománek, private communication.
22. Disorder-induced Raman scattering is observed in many forms of $sp^2$ carbon. The width of the 1347-$cm^{-1}$ peak is narrow relative to that typically seen in these other $sp^2$ carbons. Furthermore, we observe a large downshift of more than 177 100 $cm^{-1}$ for this band with decreasing excitation frequency (see Fig. 3), which has not been reported previously for other $sp^2$ carbons.
23. Strictly speaking, the concept of a diameter-dependent shift in mode frequency should be applied separately to $n$ = even and $n$ = odd tubes, because some of the mode frequencies show an abrupt change in frequency as $n$ changes by one (that is, $n$ = even to $n$ = odd), consistent with the different symmetry groups that are applicable to even and odd tubes.
24. W. Hayes and R. A. Loudon, *Light Scattering by Crystals* (Wiley, New York, 1978).
25. M. Menon, E. Richter, K. R. Subbaswamy, *J. Chem. Phys.* **104**, 5875 (1996).
26. The Kentucky group was supported by the University of Kentucky Center for Applied Energy Research and NSF grant OSR-94-52895 and DOE contract DE-F22-90PC90029. The MIT authors gratefully acknowledge NSF grant DMR95-10093 for support of this research. The work at Rice was supported by the Office of Naval Research contract N0014-91-J1794. The work at IMS was supported by the Grant-in-Aid for Scientific Research (C) 08640749 from the Japanese Ministry of Education, Science, Sports, & Culture.

28 October 1996; accepted 19 December 1996

# The Kinetic Significance of $V^{5+}$ in *n*-Butane Oxidation Catalyzed by Vanadium Phosphates

George W. Coulston,[*] Simon R. Bare, Harold Kung,
Kari Birkeland,[†] Gregory K. Bethke, Richard Harlow,
Norman Herron, Peter L. Lee

Maleic anhydride, a precursor to polyester resins, is made by oxidation of *n*-butane over vanadium phosphate catalysts. This system is of general interest because it is the only heterogeneously catalyzed, alkane-selective oxidation reaction in commercial use. Time-resolved in situ x-ray absorption spectroscopy shows that when either $\alpha_1$-$VOPO_4/SiO_2$ or $(VO)_2P_2O_7/SiO_2$ catalysts are exposed to *n*-butane, the rate of maleic anhydride formation is proportional to the rate of decay of $V^{5+}$ species in the catalyst. Thus $V^{5+}$ species are kinetically significant for the production of maleic anhydride and not just for the production of by-products. The results also suggest that $V^{5+}$ species may play a role in the initial hydrogen abstraction from *n*-butane, the rate-determining step in the reaction sequence. $V^{4+}$ sites appear to be responsible for by-product formation.

Conversion of *n*-butane to maleic anhydride, an important raw material used in polyester resin production (*1*), is the only heterogeneously catalyzed, alkane-selective oxidation reaction in commercial use. This oxide system has generated widespread interest because better understanding of the structure-property relations in the vanadium phosphate (VPO) family of materials could promote development of other selective oxidation processes. Selective oxidation reactions on reducible metal oxides are generally believed to follow the Mars and van Krevelen (*2*) mechanism. The metal oxide participates in a series of redox steps: Oxidation of an adsorbed organic molecule first reduces the metal cation, which is subsequently reoxidized either directly by gas-phase oxygen or by oxygen that has diffused through the lattice of the catalyst. At steady state, the oxide typically contains metal cations in different oxidation states, and each state plays a different role in the reaction mechanism. For the case of *n*-butane oxidation over VPOs, Bej and Rao (*3*) proposed a mechanism based on the following set of reaction steps:

$$C_4H_{10} + 14V^{5+} \rightarrow C_4H_2O_3 + 4H_2O + 14V^{4+}$$

$$C_4H_{10} + 26V^{4+} \rightarrow 4CO_2 + 5H_2O + 26V^{3+}$$

$$C_4H_2O_3 + 12V^{4+} \rightarrow 4CO_2 + H_2O + 12V^{3+}$$

$$O_2 + 4V^{3+} \rightarrow 4V^{4+}$$

$$O_2 + 4V^{4+} \rightarrow 4V^{5+}$$

The above mechanism is grossly oversimplified not only because it ignores many of the intermediates produced during *n*-butane partial oxidation to maleic anhydride (*4–6*), but also because it is not formulated with elementary reaction steps. In any case, inferring structure-performance relations based on gas-phase kinetics alone is problematic because the catalyst kinetics have not been determined.

The only detectable crystalline phase in aged industrial catalysts is vanadyl pyrophosphate, $(VO)_2P_2O_7$ (*7*), which contains $V^{4+}$ cations. Nevertheless, $VOPO_4$ ($V^{5+}$) phases have been observed in working catalysts through in situ laser Raman studies (*8, 9*). Several authors (*3, 10–12*) have speculated on the role of $V^{5+}$ centers in maleic anhydride production. Others have attributed significance to shear steps formed at the surface of $(VO)_2P_2O_7$ upon exposure of the catalyst to *n*-butane (*13*). However, in situ catalyst characterization under steady-state conditions, even when combined with reaction product analyses, is insufficient to establish the kinetic significance of an observed species. To claim a species is kinetically significant, it must at least be shown to react with a rate sufficient to support the overall rate of reaction (*14*). Such experiments require in situ monitoring of the oxide catalyst with a technique that is both fast (~1 s) and quantitative. In situ, dispersive time-resolved x-ray absorption spectroscopy (TRXAS) meets both of these criteria. In this report, we describe our approach, which combines dispersive

G. W. Coulston, R. Harlow, N. Herron, DuPont Company, Wilmington, DE 19880–0262, USA.
S. R. Bare, Dow Chemical Company, Midland, MI 48674, USA.
H. Kung, K. Birkeland, G. K. Bethke, Ipatieff Laboratory, Northwestern University, Evanston, IL 60208–3000, USA.
P. L. Lee, Materials Science Division, Argonne National Laboratory, Argonne, IL 60439, USA.

---

[*] To whom correspondence should be addressed.

[†] Present address, Dow Chemical Company, Midland, MI 48674, USA.

TRXAS, mass spectrometry (MS), dynamic feed cycling, and principal components analysis to relate maleic anhydride production directly to the presence of $V^{5+}$ centers.

The TRXAS data of $\alpha_I$-$VOPO_4/SiO_2$ (*15–22*), Fig. 1, were collected at 320°C after a step change in the gas composition from 20% $O_2$/He to *n*-butane. Singular value decomposition revealed that more than 99.998% of the variance in the data was captured by two factors. The composition profiles of $V^{5+}$ and $V^{4+}$ derived from those factors, as described above, are provided in Fig. 2A. The identification of the components as $V^{5+}$ and $V^{4+}$ is based on the position of the main absorption edge, as well as on the position of the pre-edge feature, in the corresponding reference spectra. The spectra are essentially those shown in Fig. 2D, based on analysis of data from the same sample at 380°C and discussed below. The intensities of the pre-edge features suggest $V^{5+}$ and $V^{4+}$ are in distorted octahedral environments. The first derivative of the concentration profile of $V^{5+}$ is plotted in Fig. 2B, along with the maleic anhydride MS signal. The maleic anhydride signal and the $V^{5+}$ decay profile are normalized to the respective peak rates to allow for better comparison. Clearly, the similarity between the two rate curves shows that maleic anhydride production involves the reaction of $V^{5+}$. The results also suggest that $V^{5+}$ species may play a role in the initial hydrogen abstraction from *n*-butane, which is the rate-determining step in *n*-butane selective oxidation. To see this, consider the result of a slow $V^{4+} \rightarrow V^{3+}$ reaction during hydrogen abstraction, followed by a $V^{5+} + V^{3+} \rightarrow 2V^{4+}$ reaction that is faster than the time resolution of the experiment. Although this sequence would yield only $V^{4+}$ species early in the experiment, the $V^{3+}$ concentration would be expected to increase toward the end of the experiment as the $V^{5+}$ species were depleted. However, the absence of $V^{3+}$ near the end of the experiments at 320°C suggests such a sequence is not occuring. Nonselective reactions (such as production of $CO_2$) that compete for $V^{5+}$, and lattice oxygen diffusion limitations that would result in a lower surface $V^{5+}$ concentration compared to the bulk average, could explain the slight deviation between the two response curves in Fig. 2B.

The above experiment was also performed at 380°C after reoxidizing the catalyst in 20% $O_2$/He for 30 min. In this case, three factors were found to adequately represent the data. The composition profiles and self-consistent reference spectra for this data set are shown in Fig. 2, C and D. The reference spectra suggest that $V^{3+}$ represented the additional factor. However, the data do not rule out the possibility that an isomorph of $V^{4+}$ partially contributed to the third factor, so the $V^{3+}$ concentration may actually be lower than that shown in Fig. 2C. The concentration profiles also revealed that a small amount of $V^{4+}$ remained after the initial reoxidation treatment. As observed at 320°C, maleic anhydride production ceased when $V^{5+}$ was exhausted from the catalyst. Also note that $V^{3+}$ appeared only after the $V^{5+}$ was exhausted, suggesting that reaction on $V^{4+}$ sites may lead only to by-products. Laser Raman spectroscopy (514 nm) was used to

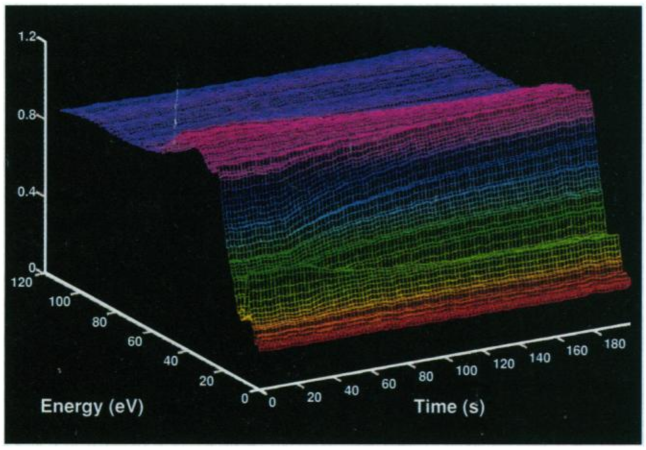

**Fig. 1.** Dispersive TRXAS during reduction at 320°C. The reactor feed concentration was changed from 20% $O_2$/He to *n*-butane at ~40 s into the experiment. Energies are measured relative to the first inflection in the K-edge absorption spectrum of V foil.

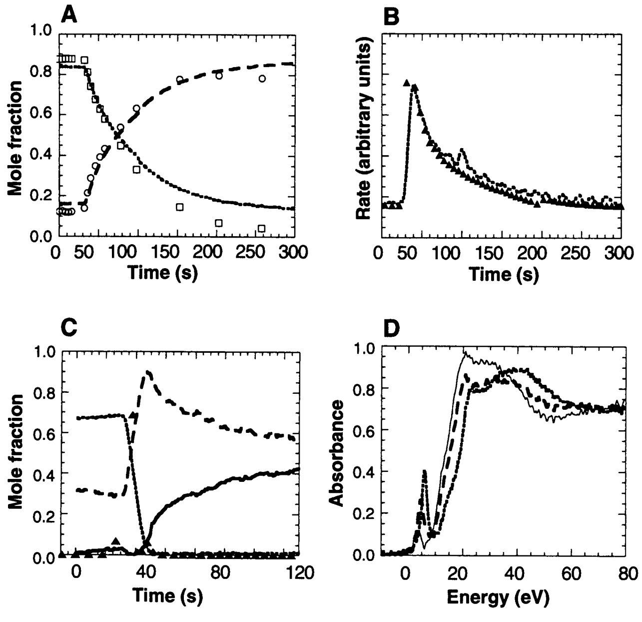

**Fig. 2.** Concentration profiles and corresponding reference spectra of $V^{5+}$ (– – –), $V^{4+}$ (— —), and $V^{3+}$ (——) determined by using principal components analysis. (**A**) Concentration profiles for reduction at 320°C. The $V^{5+}$ (□) and $V^{4+}$ (○) concentrations were determined by curve fitting with Lorentzian components. (**B**) Rate of change of the $V^{5+}$ concentration at 320°C compared to maleic anhydride production rate (△) determined by MS. (**C**) Concentration profiles for reduction at 380°C, with the maleic anhydride production rate determined by MS shown for comparison. (**D**) Principal component reference spectra corresponding to concentration profiles in (C).

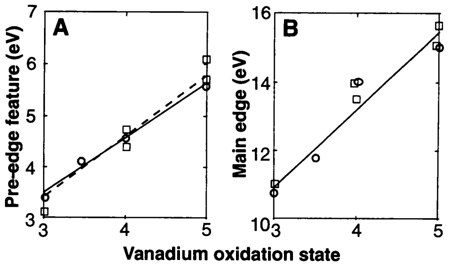

**Fig. 3.** Comparison of pre-edge (**A**) and main edge (**B**) absorption features in principal component spectra (□) to those in (*23*) (○). Energies are measured relative to the first inflection in the K-edge absorption spectrum of V foil.

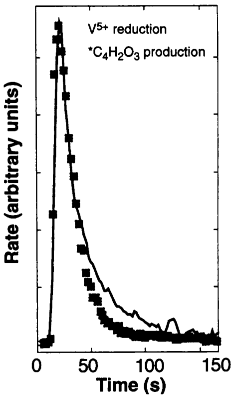

**Fig. 4.** Reaction rate of $V^{5+}$ centers in a $(VO)_2P_2O_7/SiO_2$ catalyst. The catalyst was reduced in 10% $C_4H_{10}$/Ar. The maleic anhydride production rate, as determined by MS, is also shown.

confirm that reoxidation of a similarly reduced catalyst yielded $\alpha_I$-$VOPO_4$.

We validated the self-modeling analysis with two methods: (i) Comparison of the positions of the pre-edge feature and the main absorption edge in each of the spectra generated from the self-modeling analysis with the values of those features measured for a series of vanadium oxide reference materials (*23*); and (ii) Comparison of the self-modeling composition profiles to those generated by modeling the data as a set of Lorentzians. As evident in Fig. 3, A and B, the position of the pre-edge and edge features correlated well with those collected from the reference materials. In Fig. 2A, we present the composition profiles determined for reaction at 320°C by modeling the data as a set of Lorentzians. The Lorentzian analysis and the factor analysis agree quite well. However, unlike the more traditional curve fitting, self-modeling analysis does not require reference compounds (that is, they are extracted from the data self-consistently), and the large amount of data collected in a transient dispersive XAS experiment can be handled easily.

To confirm that the above results relate to the $(VO)_2P_2O_7$ phase, we conducted similar experiments on the $(VO)_2P_2O_7/SiO_2$ catalyst. The results obtained for reduction at 380°C in 10% $C_4H_{10}/Ar$ are shown in Fig. 4. The profile for the decay of the $V^{5+}$ concentration matches well that for production of maleic anhydride, with the reaction to more completely oxidized products easily accounting for the mismatch observed at longer times.

### REFERENCES AND NOTES

1. T. R. Felthouse, J. C. Burnett, S. F. Mitchell, M. J. Mummy, *Kirk-Othmer Encyclopedia of Chemical Technology* (Wiley, New York, 1995), pp. 893–928.
2. P. Mars and D. W. v. Krevelen, *Chem. Eng. Sci.* **3**, 41 (1954).
3. S. K. Bej and M. S. Rao, *Ind. Eng. Chem. Res.* **31**, 2075 (1992).
4. F. Trifiro, *Catal. Today* **16**, 91 (1993).
5. M. Misono *et al.*, in *New Developments in Selective Oxidation*, G. Centi and F. Trifiro, Eds. (Elsevier, Amsterdam, 1990), p. 605.
6. B. Schiott and K. A. Jorgensen, *Catal. Today* **16**, 79 (1993).
7. G. Centi, *ibid.*, p. 5.
8. G. J. Hutchings, A. Desmartin-Chomel, R. Olier, J. C. Volta, *Nature* **368**, 41 (1994).
9. A. Soejarto, G. Schrader, G. S. Coulston, *Can. J. Chem. Eng.*, in press.
10. E. Bordes, *Catal. Today* **16**, 27 (1993).
11. B. K. Hodnett, *ibid.*, p. 131.
12. J. T. Ebner and M. R. Thompson, *ibid.*, p. 51.
13. P. L. Gai and K. Kourtakis, *Science* **267**, 661 (1995).
14. K. Tamaru, in *Catalysis: Science and Technology*, J. R. Anderson and M. Boudart, Eds. (Springer-Verlag, Berlin, 1991), pp. 87–129.
15. The $\alpha_I$-$VOPO_4/SiO_2$ catalyst was prepared by wet impregnation. Davisil silica (grade 644) was washed in 1 M nitric acid at 80°C for 48 hours and then rinsed repeatedly with doubly deionized water until the washings tested pH neutral. Air calcination at 90°C overnight, and subsequently at 520°C for 6 hours, removed labile hydroxyls and surface nitrates. The resulting silica had a surface area of 338 $m^2/g$ determined by the Brunauer-Emmett-Teller (BET) $N_2$ adsorption method. The silica was impregnated under conditions of incipient wetness with an aqueous solution containing ammonium metavanadate, oxalic acid, and dibasic ammonium phosphate. The solution concentrations were adjusted to obtain an elemental P:V ratio of 1:1 and a 6 weight % vanadium loading on the silica support. The P:V ratios and loading were confirmed with inductively coupled plasma-optical emission spectroscopy (ICP), and the crystalline phase was confirmed by x-ray diffraction and laser Raman spectroscopy (514 nm). The impregnated silica was dried in air at 90°C overnight at 200°C for 2 hours, and finally at 500°C for 6 hours. The resulting material had a 181-$m^2/g$ surface area. The $(VO)_2P_2O_7/SiO_2$ catalyst was prepared as follows: 10.42 g of the cluster $[(VO)_4(P_2O_7)_2(CH_3O)_4]$ $(C_{14}H_{19}N_2)_4 \cdot (CH_3OH)_4$ (*16*) was dissolved into 50 ml of dry methanol in a glove box. The deep blue solution was impregnated into 10 g silica powder (BET surface area of 300 $m^2/g$), and the slurry was evaporated to dryness. The deep blue solid was calcined in flowing air to 350°C for 1 hour and recovered for use in TRXAS experiments. The x-ray absorption and reactivity measurements were performed with a Lytle-designed in situ cell (*17*). A catalyst sample was pressed into a self-supporting wafer ~150-μm thick to keep the vanadium absorbance ~1. A small amount of unpressed catalyst was placed in the reactor next to and upstream of the wafer to enhance the MS detection of product stream maleic anhydride. This configuration satisfied the Weisz-Prater criterion (*18*), which ensures that the wafer and unpressed catalyst exhibited identical kinetics. The experiments were performed at the NSLS X6A beamline at Brookhaven National Laboratory. The x-ray optics were configured as described elsewhere (*19*), with the exception that a bent Si(111) crystal was used to access energies at the vanadium K-edge (5.46 keV). The data were analyzed with a variant of self-modeling curve resolution (*20, 21*), the details of which will be published elsewhere (*22*). Briefly, the data matrix (**D**) was factored into two subspaces related to the spectral characteristics (**S**) and composition profiles (**C**), that is, $\mathbf{D} = \mathbf{SC}$. In our approach, an initial estimate for **C** was projected into the composition subspace of the data to generate a new approximation to **C** using $\mathbf{C} = \mathbf{CUU}\dagger$, the constraint $C_{ij} > 0$ was applied, and iteration continued until the solution converged to a self-consistent set of concentration profiles and reference spectra. Singular value decomposition produced the matrix of significant right-hand eigenvectors **U**.
16. N. Herron, D. L. Thorn, R. L. Harlow, in preparation.
17. F. W. Lytle, The EXAFS Company, Pioche, NV 89043.
18. G. F. Froment and K. Bischoff, *Chemical Reactor Analysis and Design* (Wiley, New York, 1979).
19. P. L. Lee *et al.*, *Rev. Sci. Instrum.* **65**, 1 (1994).
20. E. R. Malinowski, *Factor Analysis in Chemistry* (Wiley, New York, 1991).
21. M. Fernandez-Garcia, C. M. Alvarez, G. L. Haller, *J. Phys. Chem.* **99**, 12565 (1995).
22. G. W. Coulston, in preparation.
23. J. Wong, F. W. Lytle, R. P. Messmer, D. H. Maylotte, *Phys. Rev. B* **30**, 5596 (1984).

24. We gratefully acknowledge the assistance of G. Jenning, who developed the beamline control software used in these experiments as well as J. Quintana for cutting the Si(111) crystal. This work was performed at the X6A beamline, National Synchrotron Light Source, Brookhaven National Laboratory, which is supported by the Divisions of Materials Science and Chemical Science of the U.S. Department of Energy. Work at Northwestern was supported by the Division of Chemical Sciences of DOE.

26 July 1996; accepted 17 October 1996

---

# Crustal Deformation from 1992 to 1995 at the Mid-Atlantic Ridge, Southwest Iceland, Mapped by Satellite Radar Interferometry

Hélène Vadon and Freysteinn Sigmundsson

Satellite radar interferometry observations of the Reykjanes Peninsula oblique rift in southwest Iceland show that the Reykjanes central volcano subsided at an average rate of up to 13 millimeters per year from 1992 to 1995 in response to use of its geothermal field. Interferograms spanning up to 3.12 years also include signatures of plate spreading and indicate that the plate boundary is locked at a depth of about 5 kilometers. Below that depth, the plate movements are accommodated by continuous ductile deformation, which is not fully balanced by inflow of magma from depth, causing subsidence of the plate boundary of about 6.5 millimeters per year.

The mid-ocean rift system is subaerial in Iceland, and divergent plate motion across the North American–Eurasian plate boundary (Fig. 1, inset) can be observed there by geodetic measurements, which were first attempted in 1938 (*1*). Extensive projects of distance measurements and precise leveling were initiated in Iceland in the late 1960s (*2*), and in recent years Global Positioning System (GPS) geodesy has revolutionized crustal deformation monitoring in Iceland (*3*). An area of special interest is the 50 by 25 km Reykjanes Peninsula in southwest Iceland, as it is the direct onland structural continuation of the Mid-Atlantic Ridge. The Reykjanes Peninsula plate boundary is oriented at an oblique angle to the spreading direction, not at a right angle as are typical divergent plate boundaries. The full spreading vector there is 1.86 cm/year at N103°E (*4*), whereas the average direction of the plate boundary is ~N76°E. Predicted strike-slip and opening components across the boundary are accordingly 1.7 cm/year and 0.8 cm/year. Volcanic systems along

---

H. Vadon, Centre National d'Études Spatiales, 18 Avenue Edouard Belin, 31055, Toulouse, France.
F. Sigmundsson, Nordic Volcanological Institute, University of Iceland, Grensasvegur 50, IS-108 Reykjavik, Iceland.